CHEMISTRY
A EUROPEAN JOURNAL

DOI: 10.1002/chem.200700492

Chelation-Mediated Aqueous Synthesis of Metal Oxyhydroxide and Oxide Nanostructures: Combination of Ligand-Controlled Oxidation and Ligand-Cooperative Morphogenesis

Yuya Oaki and Hiroaki Imai*[a]

Abstract: We have synthesized nanostructures of iron and cobalt oxyhydroxides and manganese oxides in aqueous solution containing a chelating agent. Nanosheets of FeOOH and Na_xMnO_2 and nanoflakes of CoOOH were generated from the corresponding divalent metal salts and ethylenediaminetetraacetate (EDTA) by one-pot synthesis under ambient conditions. The chelating agent fulfilled multiple roles in the reaction process and morphogenesis leading to two-dimensional nanostructures. Coordination to the divalent metal ions inhibited rapid precipitation of metal hydroxides and mediated oxidation to tri- and tetravalent species by dissolved oxygen. Along with the deposition, the two-dimensional and single-crystal nanostructures were also associated with interactions of the chelating agent. Therefore, this approach can be regarded as a combination of ligand-controlled oxidation and ligand-cooperative morphogenesis. Parallel control of the reaction and the morphology was achieved by a simple approach. The model cases suggest that tailoring chelation can facilitate the design of other metal oxide nanomaterials.

Keywords: aqueous synthesis · biomimetic synthesis · chelates · crystal growth · nanostructures

Introduction

Biomineralization, a classical method of materials processing, has inspired researchers to develop novel green routes. The unique structures, formation process, and properties of biominerals have been investigated in fields ranging from biology to materials science.[1] For example, the concepts of bridged crystals,[2] mesocrystals,[3] and transient amorphous phases[4] are new aspects for the understanding of biomineralization that can be applied to the synthesis of functional materials. It is widely recognized that bioinorganic materials, well-designed organic/inorganic composites, are formed by association of organic molecules and/or polymers in an aqueous medium through self-organization. Biological molecules derived from vital activities are deeply entwined in the mineralization process. However, we cannot manipulate organic molecules for designing inorganic materials like living organisms do. We believe that the key to solving this problem lies in multiple roles of organic molecules during the mineralization process.

Biomimetic synthesis of inorganic materials with tailored structures, morphologies, and properties has been explored in recent years. Control of morphology and polymorphism has been demonstrated, especially in the case of calcium carbonate.[5] These studies suggested that tailoring of appropriate organic molecules or polymers has widespread application in materials processing. Designing functional nanomaterials by biomimetic routes is a current challenge in materials science. One general concern with typical high-temperature processes is that they cause a loss of structural features on the nanoscopic scale. Although soft-solution and mild-condition routes have been reported, thermal or hydrothermal treatments and multistep processing are required in many cases. By mimicking biomineralization, simple, room-temperature, aqueous-solution processing will expand the range of materials synthesis.

In the present study, we synthesized nanostructures of iron and cobalt oxyhydroxides and manganese oxides in an aqueous solution containing divalent metal ions and a chelating agent. Neither hydrothermal treatment nor special equipment was needed in the synthetic process. The chelating agent ethylenediaminetetraacetate (EDTA) fulfilled multiple roles in the generation of nanomaterials. Chelation

[a] Dr. Y. Oaki, Prof. H. Imai
Department of Applied Chemistry
Faculty of Science and Technology
Keio University, 3-14-1 Hiyoshi
Kohoku-ku, Yokohama 223-8522 (Japan)
Fax: (+81) 45-566-1551
E-mail: hiroaki@applc.keio.ac.jp

Supporting information for this article is available on the WWW under http://www.chemeurj.org/ or from the author.

prevented the divalent metal ions M^{2+} (M = Fe, Co, Mn) from undergoing rapid precipitation of $M(OH)_2$ and mediated oxidation to tri- and/or tetravalent states to afford oxyhydroxide and oxide materials (route D in Scheme 1), while

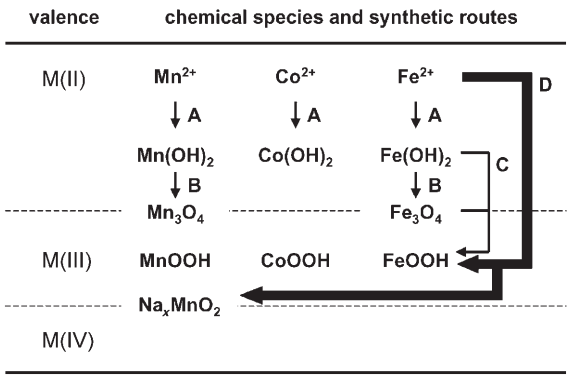

Scheme 1. Overview of synthetic routes and compounds.

conventional methods correspond to a combination of routes A and C. Moreover, the morphogenesis of two-dimensional nanostructures was also accompanied by interaction of the chelating agent. In biomineralization, various crystal forms of iron compounds, including magnetite (Fe_3O_4), goethite (α-FeOOH), lepidocrocite (γ-FeOOH), and ferrihydrite, are selectively produced under certain conditions.[1a,6] Compared to other biominerals, such as carbonates and phosphates, the oxidation state of iron is exactly controlled in an aqueous medium under ambient conditions, as were morphology and size of the crystals. We also controlled both the morphology and the oxidation sate of metal ions by one-pot biomimetic synthesis in aqueous solution. In other words, the ligand was involved in both controlled oxidation and cooperative morphogenesis. Parallel control of the reaction and morphology is a significant technique for biomimetic crystal design of metal oxides. Furthermore, coordination between metal ions and organic ligands can be predicted from the large body of research available in coordination chemistry. The chelation-mediated approach will be applied to other systems to give functional nanomaterials. The synthesis of iron (goethite, α-FeOOH) and cobalt oxyhydroxides (heterogenite, CoOOH) and manganese oxide (birnessite, Na_xMnO_2) and oxyhydroxide (feiktnechtite, β-MnOOH) are presented below, after which mutual formation mechanisms are discussed.

Abstract in Japanese:

有機分子の配位によって、水溶液中における酸化反応と形態形成を同時に制御することで、ワンポットで金属オキシ水酸化物および酸化物ナノシートを合成することに成功した。常温・常圧の水溶液中において、典型的なキレート試薬であるEDTAを用い、厚さ10 nm前後の鉄・コバルト・マンガンの酸化物ナノシートを合成し、それらの構造の評価および形成プロセスについて検討を行った。EDTAと二価の金属イオンの錯形成により、水酸化物の沈殿生成が抑制され、溶存酸素による三価もしくは四価への酸化反応が進行し、オキシ水酸化物および酸化物の析出がおこる。同時に、EDTAが生成物の特異的な面に吸着することにより、ナノシート構造が誘導されたと考えられる。キレート試薬と金属イオンの組み合わせを考慮することで、種々のセラミックスナノ材料の室温・溶液プロセスでの合成および形態のデザイン、さらにはその機能化が期待できる。

Results and Discussion

Iron oxyhydroxide nanosheets: The synthesis of goethite has long been studied, especially in colloid chemistry, because of its scientific and technological importance.[7–11] In a typical method, acicular goethite was obtained from trivalent iron precursors (Fe^{3+}) by mixing with an alkaline solution.[7–10] The hydrothermal reaction resulted in the formation of hematite nanostructures under certain conditions.[12] Although a divalent iron salt (Fe^{2+}) was adopted in some cases, the formation of goethite was followed by the oxidation of hydroxide in the initial precipitate (routes A and C in Scheme 1).[11] We generated goethite nanosheets from divalent Fe^{2+} and EDTA without an oxidizing reagent and air flow (route D in Scheme 1). Moreover, to the best of our knowledge, there have been no reports on the formation of a sheetlike morphology of goethite.

Precursor solutions containing 20 mM of $FeCl_2 \cdot 4H_2O$ and 20 or 50 mM of EDTA were prepared in purified water at room temperature. An equal volume of 200 mM sodium hydroxide solution was added to the precursor solution without stirring, and the mixture was maintained at 25 °C. After three days, the precipitate was collected by centrifugation and washed with purified water. The morphology was observed under a field-emission scanning electron microscope (FESEM) and a field-emission transmission electron microscope (FETEM). The FETEM analysis was performed by the following means: high-resolution (HRTEM) image and its fast-Fourier transform (FFT) image, energy-dispersive X-ray analysis (EDX), selected-area electron diffraction (SAED), and high-angle annular dark-field scanning transmission electron microscopy (HAADF-STEM). The crystal structure was characterized by X-ray diffraction (XRD) with $2\theta/\theta$ scanning. The interaction of EDTA was monitored with a UV/Vis spectrophotometer and by FTIR spectroscopy.

The reaction started on mixing the solutions containing Fe^{2+}/EDTA and NaOH. The transparent, yellowish green solution immediately changed to a dark orange liquid on mixing. The structure and morphology of the product were not dependent on the initial EDTA concentration. The XRD pattern characterized the resultant precipitate as goethite (α-FeOOH) containing Fe^{3+} (Figure 1a). In contrast, magnetite (Fe_3O_4), which contains both Fe^{II} and Fe^{III} irons, was obtained via $Fe^{II}(OH)_2$ in the absence of EDTA (see Figure S1 in the Supporting Information). The FESEM images show that the goethite had a sheetlike morphology consisting of nanofibrils (Figure 1b–e). According to FESEM and FETEM observations, the ranges of width and length of the nanosheets were respectively 50–500 and 500–

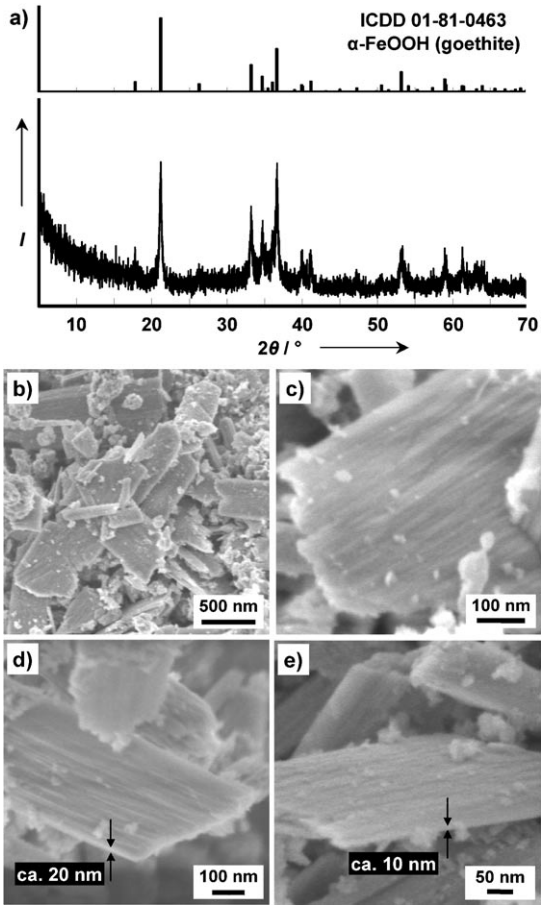

Figure 1. Structure and morphology of FeOOH nanosheets. a) XRD pattern of the precipitate (lower panel) and peak positions in the ICDD card (upper panel). b and c) FESEM images of goethite nanosheets consisting of nanofibrils. d and e) Magnified FESEM images viewed in the thickness direction.

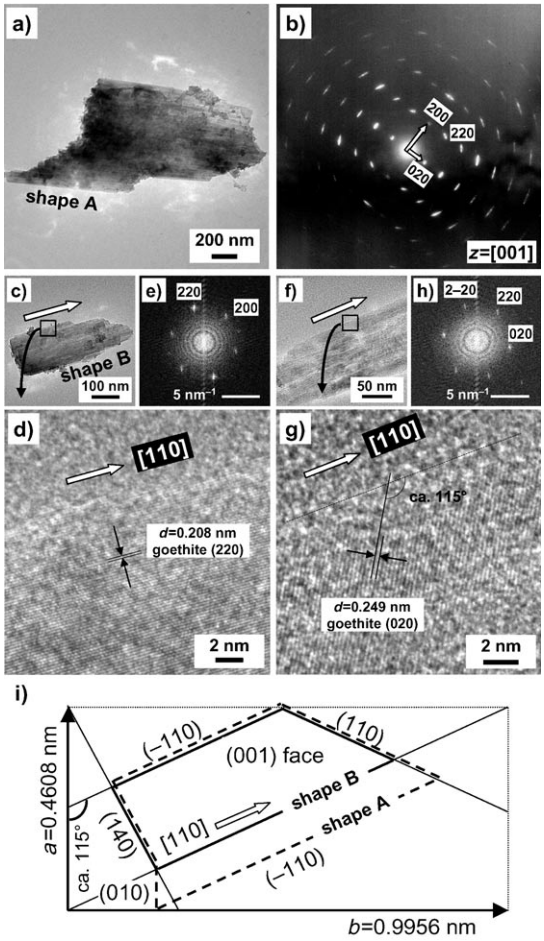

Figure 2. FETEM analysis of the goethite nanosheets. a) and b) Bright-field FETEM image and SAED pattern taken in the [001] direction, indicating that the nanosheet is a single crystalline material spread over the (001) plane. c) and d) FETEM and HRTEM images showing the lattice spacing of the (220) plane parallel to the edge. e) FFT image of panel d). f and g) FETEM and HRTEM images showing the lattice spacing of the (020) plane with a dihedral angle of about 115°. h) FFT image of panel g). i) Morphology and growth direction of the goethite nanosheet viewed in the [001] direction, estimated from the structure of the unit cell. Shapes A and B represent the morphologies shown in the FETEM images in a) and c), respectively.

2000 nm, and the thickness was less than 20 nm (Figure 1b–e and Figure 2a).

The spotted SAED pattern suggested that the nanosheet with a fibrous interior had a single-crystalline structure spread over the (001) plane (Figure 2a and b). According to HRTEM observations, the lattice spacing corresponding to the (110) plane was observed on the edge parallel to the longitudinal direction (Figure 2c–e). The (020) plane was recognized in the elongated direction with a dihedral angle of about 115° (Figure 2f–h). This suggests that the nanosheets display a (001) face and are elongated in the [010] direction. The sides of the sheet were assigned to the (110), (140), and (010) faces from HRTEM, FFT, and the dihedral angles in the image. Therefore, the growth direction of a nanosheet is as illustrated in Figure 2i. In addition to the nanosheets, spherical aggregates of tiny flakes were observed in the same precipitate (Figure 3a and b). When the electron beam was perpendicular to the spheres, the SAED pattern showed Debye–Scherrer rings assigned to the (040), (200), (220), and (060) planes of goethite (Figure 3a and b). The *c* axis was perpendicular to the flakes, whereas the *a* and *b* axes were not arranged in the same crystallographic direction. In rare cases, small amounts of thinner and larger nanosheets were also present in the precipitate (Figure 3c and d). Although selective morphosynthesis was not achieved in this study, optimization of the synthetic condition should realize morphological control of these nanostructures. In contrast, these characteristic morphologies were not observed when trivalent iron salts ($FeCl_3$) were used instead of $FeCl_2 \cdot 4H_2O$ (Figure S2 in the Supporting Information).

During the synthetic process, EDTA played important roles in the generation of goethite nanosheets. The interaction of EDTA was investigated by UV/Vis and FTIR analysis. Figure 4a shows UV/Vis spectra of precursor solutions without and with EDTA. The yellowish green color of the Fe^{2+} solution deepened after addition of EDTA. A strong absorption band appeared around 255 nm in the diluted pre-

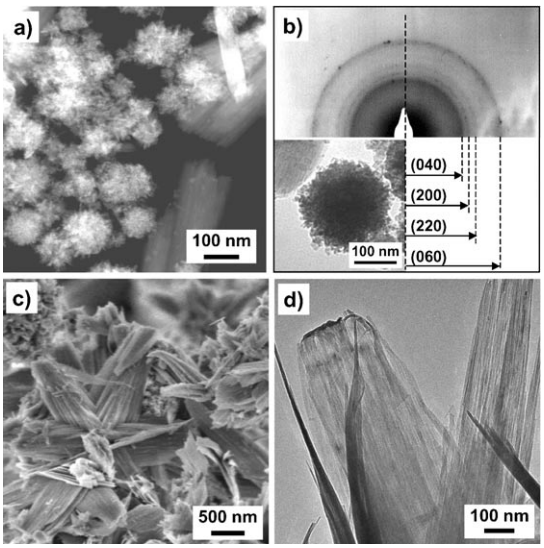

Figure 3. FESEM and FETEM images of goethite nanostructures other than sheets. a) HAADF-STEM image of spherical aggregates made of tiny nanoflakes. b) Bright-field image and SAED pattern; c) and d) FESEM and FETEM images of the larger and thinner nanosheets contained in the precipitates, respectively.

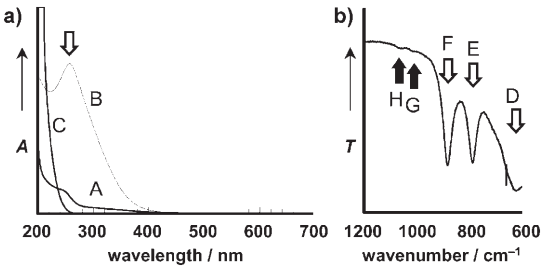

Figure 4. UV/Vis and FTIR spectra of the precursor solutions and the FeOOH nanosheets, respectively. a) UV/Vis spectra of the precursor solutions (A: 20 mM aqueous Fe^{2+} solution; B: precursor solution containing 20 mM of Fe^{2+} and 50 mM of EDTA; C: 20 mM aqueous EDTA solution as reference). Spectrum B was obtained from a precursor solution diluted with water to 2%. b) FTIR spectrum of the goethite nanosheets (D: Fe–O stretching band;[8b,9b] E and F: Fe-O-H bending mode, in- and out-of-plane, respectively;[8b,9b] G and H: C–N stretching mode of residual EDTA).

cursor solution containing Fe^{2+} and EDTA. In contrast, an aqueous solution of EDTA did not show an absorption peak at this wavelength, which can be attributed to chelation between Fe^{2+} and EDTA.[13] This implies that chelation inhibited precipitation of hydroxide. The FTIR spectrum of the resultant precipitate shows the weak absorption peaks resulting from the amino groups of EDTA around 1050 cm^{-1} (Figure 4b). Therefore, EDTA was involved in the morphogenesis of nanosheets as well as the reaction process.

Cobalt oxyhydroxide nanoflakes: Cobalt-related materials have been investigated for application in electrochemical devices such as capacitors.[14–18] Sodium cobalt oxide has been reported to have superconductive properties.[19] The conventional synthetic route is the oxidation of Co^{II} hydroxide or acetate species.[14,16a,17] Direct deposition was demonstrated under flowing oxygen or ozone.[16b,18] In the present study, we fabricated CoOOH nanoflakes from divalent Co^{2+} and EDTA by one-pot synthesis. The experimental conditions for the CoOOH nanoflakes were almost the same as those for goethite, except that the initial EDTA concentration and reaction time were set to 20 mM and five days.

A transparent pink solution containing Co^{2+} and EDTA changed to a red-purple color on mixing with NaOH. After five days, the dark brownish precipitate was collected by centrifugation. The XRD pattern indicated that the presence of EDTA led to formation of CoOOH (heterogenite) containing Co^{3+} (Figure 5a). Figure 5b and c show FESEM images of the CoOOH nanoflakes, which are less than 5 nm in thickness. In contrast, hexagonal plates of β-$Co(OH)_2$ were preferentially produced in the precursor solution without EDTA (see Figure S3 in the Supporting Information). Several FETEM and HAADF-STEM images showed the CoOOH nanoflakes to be approximately 100 nm in size, and the edges were partially rolled up due to their thinness (Figure 6a–c). A rolled morphology of a cobalt compound is rare, although similar phenomena have been observed in exfoliated nanosheets of various metal oxides.[20] When the electron beam was perpendicular to several flakes, the SAED pattern showed broken Debye–Scherrer rings corresponding to the (100) and (110) planes of a brucite-type structure (Figure 6c and d). Thus, the nanoflakes were oriented perpendicular to the *c* axis. Since the nanoscale interior was not recognized in the FETEM images (Figure 6a–c), the flake is regarded as a single crystal spread over the

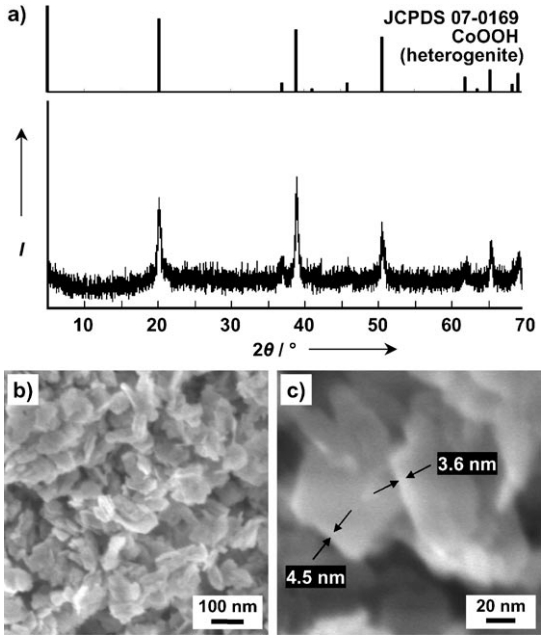

Figure 5. Structure and morphology of the CoOOH nanoflakes. a) XRD pattern of the precipitate (lower panel) and peak positions in the JCPDS card (upper panel). b) FESEM image of the CoOOH nanoflakes. c) Magnified FESEM images showing the thickness.

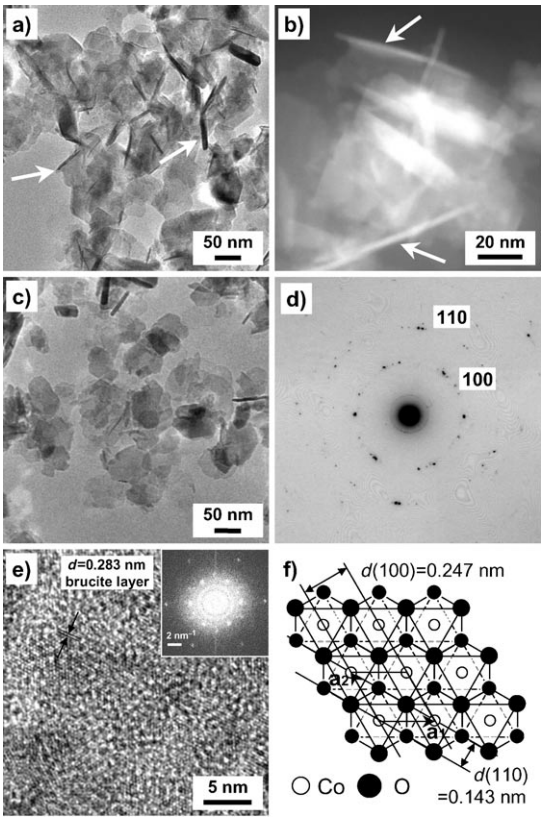

Figure 6. FETEM analysis of the CoOOH nanoflakes. a) and b) FETEM and HAADF-STEM images of the nanoflakes, respectively. The white arrows indicate the rolled-up morphology. c) and d) FETEM image and SAED pattern, respectively. e) HRTEM and its FFT image (inset). f) Schematic model of the brucite-type monolayer consisting of CoO_6 octahedra.

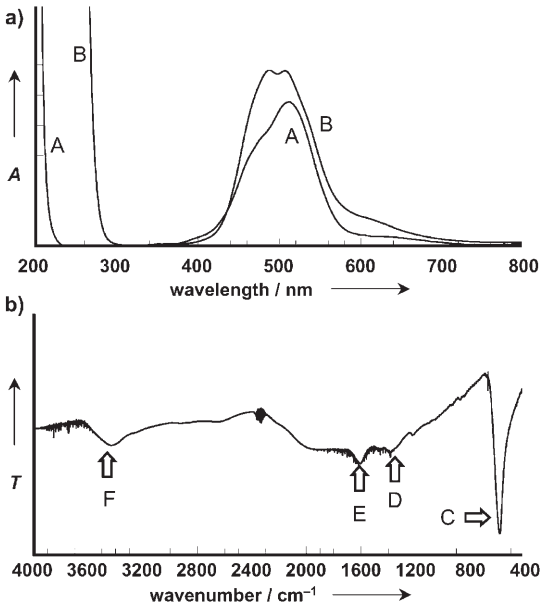

Figure 7. UV/Vis and FTIR spectra of the precursor solutions and the CoOOH nanoflakes, respectively. a) UV/Vis spectra of the precursor solutions (A: 20 mM aqueous Co^{2+} solution; B: precursor solution containing 20 mM of Co^{2+} and 50 mM of EDTA). b) FTIR spectrum of the CoOOH nanoflakes: C: Co–O stretching band; D and E: absorption resulting from included carbonate ions and the adsorbed water molecules; F: O–H stretching vibration in the interlayer space of the brucite-type structure. The absorption peaks assignable to residual EDTA were not recognized in the spectrum.

(001) plane. The HRTEM image and its FFT indicate that the nanoflakes were constructed from brucite-type layers having $Co^{III}O_6$ octahedral units (Figure 6e and f).

Changes in UV/Vis absorption suggest coordination between Co^{2+} and EDTA in the precursor solution (Figure 7a). An absorption band below 300 nm, a peak centered at 487 nm, and a shoulder around 600 nm appeared on mixing of Co^{2+} and EDTA. In accordance with previous studies in coordination chemistry, EDTA having two amine and four carboxylate groups can form a complex with the Co^{2+} ion and cause the UV/Vis spectroscopic changes. Residual EDTA molecules were not clearly detected by FTIR analysis of the precipitate (Figure 7b). It is assumed that the adsorbed EDTA would be removed during washing and centrifugation.

Manganese oxide nanosheets: Manganese oxides have a wide variety of applications originating from their crystal structures, such as catalysis and electrochemical devices.[21–25] Among the several types of manganese oxides, birnessite has attracted much interest because of its catalytic and electrochemical properties.[21] It has been reported that various crystal structures are derived from birnessite through hydrothermal treatment under certain conditions.[25] Three typical routes are used to obtain birnessite: air or chemical oxidation of Mn^{2+} and $Mn(OH)_2$, reduction of MnO_4^-, and redox reaction of Mn^{2+} and MnO_4^-. We generated birnessite nanosheets from divalent manganese ions by association with EDTA. The basic idea and experimental procedure were the same as for the FeOOH and CoOOH nanostructures. Figure 8 shows the structure and morphology of birnessite nanosheets. The XRD pattern indicates that the main product is a birnessite-type manganese oxide, even though a small amount of β-MnOOH (feiktnechtite) was contained (Figure 8a). The FESEM images show flexible nanosheets that are several micrometers in size and less than 10 nm in thickness (Figure 8b and c). The nanosheets are oriented perpendicular to *c* axis, while the *a* and *b* axes were not arranged in the same direction (Figure 8d and e). The detailed characterization and analysis of the birnessite nanosheets were described in our previous report.[26]

Synthetic route of the chelation-mediated approach: We synthesized FeOOH, CoOOH, and Na_xMnO_2 nanostructures through a simple chelation-mediated approach. Scheme 1 summarizes the synthetic routes, including the oxidation states and compounds. In conventional methods, mixing of a divalent metal salt and alkaline solutions results in rapid precipitation of $M^{II}(OH)_2$ and/or $M^{II,III}{}_3O_4$ species under ambient conditions (routes A and/or B in Scheme 1). The divalent $M^{II}(OH)_2$ species are easily oxidized to $M^{II/III}{}_3O_4$ by aging or drying, except in the case of cobalt.[27] However,

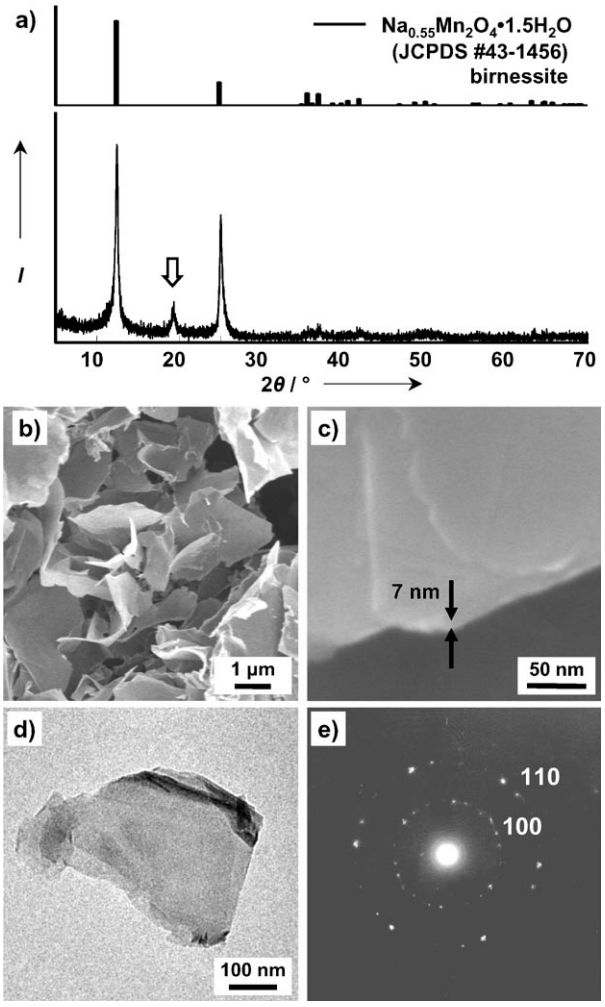

Figure 8. Structure and morphology of the birnessite nanosheets. a) XRD pattern of the precipitate (lower panel) and peak positions in the JCPDS card (upper panel). The peak denoted by a white arrow is assignable to β-MnOOH. b) and c) FESEM images of nanosheets about 7 nm in thickness. d) and e) FETEM image and SAED pattern, respectively.

the oxidation state did not completely change to from M^{II} M^{III} without any treatment. Air or chemical oxidation is required for the preparation of oxyhydroxides and/or oxides from the precursor solution and initial precipitate (routes A and C in Scheme 1). Although various methods were demonstrated in earlier studies, morphological control was difficult in the two-step routes including precipitation and oxidation. Our chelation-mediated approach led to the oxyhydroxide and oxide via one-pot synthesis (route D in Scheme 1).

Proposed model for the control of reaction: We infer that the coordination between metal species and EDTA as a ligand (L) is involved in both the reaction process and the morphogenesis of two-dimensional nanostructures. Scheme 2 summarizes the reaction process. The chelation between M^{2+} and L in the precursor solutions prevents deposition of $M^{II}(OH)_2$ even after addition of an alkaline solu-

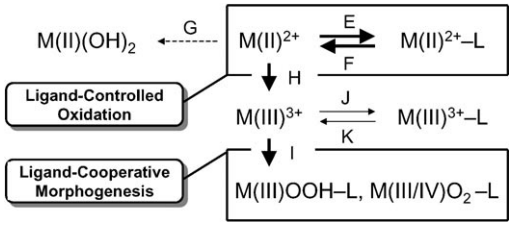

Scheme 2. Synthetic routes involving the ligand and oxidation states of metal ions.

tion. The M^{2+} preferentially coordinate with the ligands (route E in Scheme 2) rather than hydroxide ions (route G in Scheme 2). However, dissolved M^{2+} species were also present owing to the equilibrium between M^{2+} and M^{2+}-L (routes E and F in Scheme 2). Without the ligand the dissolved M^{II} species would be oxidized to M^{III} by dissolved oxygen under alkaline condition (route H in Scheme 2). When the ligands are coordinated to M^{2+}, it may be difficult to change the oxidation state of M^{II}. In this way, "ligand-controlled oxidation" is accomplished in aqueous solution (routes F and H in Scheme 2). The oxidized species would form oxyhydroxide or oxide precipitates because of their low solubility (route I in Scheme 2), even though equilibrium between M^{3+} and M^{3+}-L is possible in solution (routes J and K in Scheme 2). In this case, M^{3+} preferentially provided oxyhydroxide and oxide precipitates rather than the complex with the ligand as dissolved species. While the conventional methods are regarded as a solid-state phase transitions, our ligand-controlled oxidation process is a direct route to oxyhydroxide and oxide materials in an aqueous solution.

Although the reaction mechanism including chelation and oxidation remains unclear, the model is partially supported in earlier works. Precipitates of $Co(OH)_2$ and $Co(OH)_{2-x}(CH_3COO)_x$ were gradually transformed into CoOOH through dissolution and reprecipitation in a KOH solution because Co^{3+} is more stable than Co^{2+} under alkaline conditions.[14,16a] Therefore, the direct deposition of CoOOH would be expected in our ligand-controlled oxidation process because of the alkaline conditions. In the FeOOH system, the activity of Fe^{3+} $a_{(Fe3+)}$ ions was estimated from the solubility products K_{sp} and pH in the solution.[28] Since the pH was roughly constant, with a range of 12.5–13.0 before and after deposition of FeOOH, $a_{(Fe3+)}$ was calculated to be approximately 10^{-37} M in our experiment on the basis of the following equation [Eq. (1)[28]].

$$\lg a_{(Fe3+)} = \lg K_{sp} - 3\,pH \quad (1)$$

The lower solubility of Fe^{3+} results in formation of FeOOH even though chelation between Fe^{3+} and the ligand was not considered in the calculation. As a consequence, the chelation between M^{2+} and EDTA inhibits the precipitation of hydroxides and simultaneously mediates oxidation to M^{3+}, which provides the oxyhydroxide and oxide. Further investi-

gation with regard to monitoring the chelation and oxidation behaviors is needed for a thorough understanding of the reaction process. Moreover, the coordination behavior between metal ions and ligands determines the controllability of the reaction process.

Proposed model for morphological control: Since the two-dimensional and single-crystalline nanostructures were associated with specific interactions of EDTA molecules, the crystal growth can be regarded as ligand-cooperative morphogenesis. The ligand itself and/or M^{3+}-L complex interacts with a specific crystal surface. Residual EDTA was detected only in the case of FeOOH, and the corresponding absorption peaks were very weak in the FTIR spectrum. The EDTA was easily removed by washing with water. Thus, the chelating agent contributed to the formation of single-crystalline and two-dimensional morphologies through specific interaction as well as to the reaction process.

On the other hand, we have reported that nanocrystalline mosaics are formed by incorporation of organic polymers in biominerals and biomimetic architectures.[2,29] Birnessite-type manganese oxide and cobalt hydroxide nanoflakes with mosaic interior were synthesized in an aqueous solution containing poly(acrylic acid) and polyethyleneimine, respectively.[29d] It is generally known that adsorption of polymeric species is irreversible and strong, while that of small molecules is reversible and weak. Thus, the formation of either mosaic or single-crystalline structures was determined by the adsorbability of the molecules. The nanocrystalline mosaics were generated by strong and irreversible adsorption of polymers.[29] In contrast, single-crystalline structures are obtained by reversible and relatively weak interaction of small molecules, and specific adsorption on crystal faces leads to two-dimensional morphologies.

Conclusion

We have generated metal oxyhydroxide and oxide nanostructures by a chelation-mediated approach in aqueous solution. Parallel control of the reaction and the morphology of $Fe^{III}OOH$, $Co^{III}OOH$, and $Na_xMn^{III,IV}O_2$ was achieved by EDTA. Chelation between M^{2+} and EDTA inhibited precipitation of $M^{II}(OH)_2$ and simultaneously mediated oxidation to M^{3+} by dissolved oxygen without oxidizing agents or an air flow. The specific interaction led to the generation of two-dimensional and single-crystalline nanostructures. The combination of ligand-controlled oxidation and ligand-cooperative morphogenesis resulted in a one-pot synthesis of metal oxyhydroxide and oxide nanostructures in aqueous solution. A similar strategy may underlie biomineralization, as parallel control of the crystal structure, morphology, and oxidation state of metals has been achieved in biogenic iron compounds.

The synthetic pathway is beneficial for technological applications because the residual organic compound can be removed, which is not possible with polymers. Combination with hydrothermal processing will create various functional oxides, such as Fe_2O_3 and MnO_2. Among various applications of iron-, cobalt-, and manganese-related materials, the nanoscopic architectures can be advantageous for electrochemical devices such as electrodes for lithium ion batteries and electrochemical capacitors.

Furthermore, the simple chelation-mediated approach can be widely applied in materials synthesis. We adopted EDTA, a simple chelating agent, in this model study to demonstrate the basic idea. The chemical affinity between a chelating agent and metal ions is predictable, as shown in previous studies in complex and aquatic chemistry. In accordance with the molecular structure, the ligand plays important roles in the reaction and morphogenesis. The coordination behavior controls the reaction, and the adsorbability on crystals induces morphological control. Therefore, molecular design is required for further development of the approach.

Experimental Section

Materials and procedures

Iron oxyhydroxide: Stock solutions containing 20 or 50 mM of disodium dihydrogen ethylenediaminetetraacetate (EDTA, Kanto Chemical, 99.5%) were prepared in polystyrene or polypropylene vessels with purified water at room temperature. Then, 20 mM of $FeCl_2{\cdot}4H_2O$ (Kanto Chemical, 99.0%) was dissolved in the stock solution. Then, an equal volume of 200 mM sodium hydroxide (NaOH, Junsei Chemical, 96.0%) was added to the precursor solution without stirring. The sealed sample bottles were maintained at 25 °C for three days. The resultant precipitates were collected by centrifugation, rinsed with purified water several times, and dried at 25 °C.

Cobalt oxyhydroxide: The procedure was the same as for iron oxyhydroxide except for the following conditions. The precursor solutions contained 20 mM of EDTA and 20 mM of $CoCl_2{\cdot}6H_2O$ (Kanto Chemical, 99.0%). After adding NaOH, the reaction mixture was left for five days at 25 °C. In this case, the precipitates were prepared from 500 mL of the precursor solution in three polystyrene bottles.

Manganese oxide: The procedure was the same as that of iron oxyhydroxide except for the following conditions. The precursor solutions contained 20 mM of EDTA and 20 mM of $MnCl_2{\cdot}4H_2O$ (Kanto Chemical, 99.0%). After adding NaOH, the reaction mixture was left for three or five days at 25 °C. However, the reaction time did not influence the structure and morphology of the resultant birnessite nanosheets.[26]

Characterization: Morphologies were observed by FESEM (FEI Sirion operated at 2.0 kV), FETEM (FEI, Tecnai F20 operated at 200 kV), and TEM (FEI Tecnai G2 Spirit operated at 120 kV) without any conductive treatment. The following analyses was performed in FETEM studies: HRTEM, SAED, HAADF-STEM, and EDX (EDAX, r-TEM 32). For FETEM observations, a copper grid with a supported collodion membrane was immersed in the nanosheet colloid. In another method, the colloidal liquid containing the nanostructures was prepared in purified water by using an ultrasonic bath. The crystal structure was analyzed by XRD (Bruker AXS, D8 Advance, $Cu_{K\alpha}$ radiation, equipped with a graphite monochromator). All samples were measured in $2\theta/\theta$ scanning mode and triple integration under ambient condition. Residual organic compound was analyzed by FTIR (Bio-Rad FTS-60A, KBr method). The UV/Vis spectra resulting from complexation between metal ions and EDTA were monitored by a spectrophotometer at room temperature (JASCO, V-560).

Acknowledgements

This work was supported by the 21st Century COE program "KEIO Life Conjugated Chemistry" from the Ministry of Education, Culture, Sports, Science, and Technology, Japan and the Murata Science Foundation. Y.O. is grateful to have received the JSPS research fellowship for young scientists.

[1] a) S. Mann, *Biomineralization* (Eds.: R. G. Compton, S. G. Davies, J. Evans), Oxford University Press, Oxford, **2001**; b) S. Weiner, L. Addadi, *J. Mater. Chem.* **1997**, *7*, 689–702; c) T. Kato, *Adv. Mater.* **2000**, *12*, 1543–1546.

[2] a) Y. Oaki, A. Kotachi, T. Miura, H. Imai, *Adv. Funct. Mater.* **2006**, *16*, 1633–1639; b) Y. Oaki, H. Imai, *Small* **2006**, *2*, 66–70; c) H. Imai, Y. Oaki, A. Kotachi, *Bull. Chem. Soc. Jpn.* **2007**, *80*, 1834–1851.

[3] a) M. Niederberger, H. Cölfen, *Phys. Chem. Chem. Phys.* **2006**, *8*, 3271–3287; b) H. Cölfen, M. Antonietti, *Angew. Chem.* **2005**, *117*, 5714–5730; *Angew. Chem. Int. Ed.* **2005**, *44*, 5576–5591; c) H. Cölfen, S. Mann, *Angew. Chem.* **2003**, *115*, 2452–2468; *Angew. Chem. Int. Ed.* **2003**, *42*, 2350–2365, and references therein.

[4] L. Addadi, S. Raz, S. Weiner, *Adv. Mater.* **2003**, *15*, 959–970.

[5] S. H. Yu, H. Cölfen, *J. Mater. Chem.* **2004**, *14*, 2124–2147.

[6] a) T. Matsunaga, Y. Okamura, T. Tanaka, *J. Mater. Chem.* **2004**, *14*, 2099–2105; b) J. F. Banfield, S. A. Welch, H. Zhang, T. T. Ebert, R. L. Penn, *Science* **2000**, *289*, 751–754; c) J. L. Jambor, J. E. Dutrizac, *Chem. Rev.* **1998**, *98*, 2549–2585, and references therein.

[7] M. Kosmulski, S. Durand-Vidal, E. Maczka, J. B. Rosenholm, *J. Colloid Interface Sci.* **2004**, *271*, 261–269, and references therein.

[8] a) C. Sudakar, G. N. Subbanna, T. R. N. Kutty, *J. Mater. Chem.* **2002**, *12*, 107–116; b) C. Sudakar, G. N. Subbanna, T. R. N. Kutty, *J. Mater. Sci.* **2004**, *39*, 4271–4286.

[9] a) L. C. Varanda, M. P. Morales, M. Jafelicci, Jr., C. J. Serna, *J. Mater. Chem.* **2002**, *12*, 3649–3653; b) N. O. Nunez, M. P. Moraies, P. Tartaj, C. J. Serna, *J. Mater. Chem.* **2000**, *10*, 2561–2565.

[10] R. L. Penn, J. J. Erbs, D. M. Gulliver, *J. Cryst. Growth* **2006**, *293*, 1–4.

[11] a) T. F. Barton, T. Price, K. Becker, J. G. Dillard, *Colloid Surfaces* **1991**, *53*, 209–222; b) J. Subrt, L. Perez-Maqueda, J. M. Criado, C. Real, J. Bohacek, E. Vecernikova, *J. Am. Ceram. Soc.* **2000**, *83*, 294–298.

[12] a) M. Ozaki, N. Ookoshi, E. Matijevic, *J. Colloid Interface Sci.* **1990**, *137*, 546–549; b) T. Sugimoto, Y. Wang, H. Itoh, A. Muramatsu, *Colloids Surf.* **1998**, *134*, 265–279; c) M. Niederberger, F. Krumeich, K. Hegetschweiler, R. Nesper, *Chem. Mater.* **2002**, *14*, 78–82; d) M. Cao, T. Liu, S. Gao, G. Sun, X. Wu, C. Hu, Z. L. Wang, *Angew. Chem.* **2005**, *117*, 4269–4273; *Angew. Chem. Int. Ed.* **2005**, *44*, 4197–4201; e) Y. M. Zhao, Y. H. Li, R. Z. Ma, M. J. Roe, D. G. McCartney, Y. Q. Zhu, *Small* **2006**, *2*, 422–427.

[13] A. B. P. Lever, *Inorganic Electronic Spectroscopy*, 2nd ed., **1984**, Elsevier, Amsterdam, Chap. 6.

[14] E. Hosono, S. Fujihara, I. Honma, M. Ichihara, H. Zhou, *J. Power Sources* **2006**, *158*, 779–783.

[15] R. J. Wu, J. G. Wu, T. K. Tsai, C. T. Yeh, *Sensors Actuators B* **2006**, *120*, 104–109.

[16] a) V. Pralong, A. Delahaye-Vidal, B. Beaudoin, B. Gerand, J. M. Tarascon, *J. Mater. Chem.* **1999**, *9*, 955–960; b) F. Barde, M. R. Palacin, B. Beaudoin, A. Delahaye-Vidal, J. M. Tarascon, *Chem. Mater.* **2004**, *16*, 299–306.

[17] R. L. Penn, A. T. Stone, D. R. Veblen, *J. Phys. Chem. B* **2001**, *105*, 4690–4697.

[18] a) M. Figlarz, J. Guenot, F. Fievet-Vincent, *J. Mater. Sci.* **1976**, *11*, 2267–2270; b) Y. Zhu, H. Li, Y. Koltypin, A. Gedanken, *J. Mater. Chem.* **2002**, *12*, 729–733.

[19] K. Takada, H. Sakurai, E. Takayama-Muromachi, F. Izumi, R. A. Dilanian, T. Sasaki, *Nature* **2003**, *422*, 53.

[20] a) R. Ma, Y. Bando, T. Sasaki, *J. Phys. Chem. B* **2004**, *108*, 2115–2119; b) T. Sasaki, *J. Ceram. Soc. Jpn.* **2007**, *115*, 9–16, and references therein.

[21] Q. Feng, H. Kanoh, K. Ooi, *J. Mater. Chem.* **1999**, *9*, 319–333, and references therein.

[22] a) J. Cai, J. Liu, S. L. Suib, *Chem. Mater.* **2002**, *14*, 2071–2077; b) S. L. Brock, M. Sanabria, S. L. Suib, V. Urban, P. Thiyagarajan, D. I. Potter, *J. Phys. Chem. B* **1999**, *103*, 7416–7428; c) J. Luo, A. Huang, S. H. Park, S. L. Suib, C.-L. O'Young, *Chem. Mater.* **1998**, *10*, 1561–1568; d) Q. Gao, O. Giraldo, W. Tong, S. L. Suib, *Chem. Mater.* **2001**, *13*, 778–786.

[23] a) L. Wang, K. Takada, A. Kajiyama, M. Onoda, Y. Michiue, L. Zhang, M. Watanabe, T. Sasaki, *Chem. Mater.* **2003**, *15*, 4508–4514; b) Y. Omomo, T. Sasaki, L. Wang, M. Watanabe, *J. Am. Chem. Soc.* **2003**, *125*, 3568–3575.

[24] a) X. Yang, Y. Makita, Z.-H. Liu, K. Sakane, K. Ooi, *Chem. Mater.* **2004**, *16*, 5581–5588; b) Q. Feng, L. Liu, K. Yanagisawa, *J. Mater. Sci.* **2000**, *35*, 1567–1570.

[25] Q. Feng, K. Yanagisawa, N. Yamasaki, *Chem. Commun.* **1996**, 1607–1608.

[26] Y. Oaki, H. Imai, *Angew. Chem.* **2007**, *119*, 5039–5043; *Angew. Chem. Int. Ed*. **2007**, *46*, 4951–4955.

[27] a) For iron oxide: M. Kiyama, *Bull. Chem. Soc. Jpn.* **1974**, *47*, 1646–1650; for manganese oxide: b) A. R. Nichols, Jr., J. H. Walton, *J. Am. Chem. Soc.* **1942**, *64*, 1866–1870.

[28] R. M. Cornell, U. Schwertmann, *The Iron Oxides*, **2003**, Wiley-VCH, Weinheim, Germany, Chap. 9.

[29] a) Y. Oaki, H. Imai, *Angew. Chem.* **2005**, *117*, 6729–6733; *Angew. Chem. Int. Ed.* **2005**, *44*, 6571–6575; b) Y. Oaki, H. Imai, *Adv. Funct. Mater.* **2005**, *15*, 1407–1414; c) Y. Oaki, H. Imai, *Chem. Commun.* **2005**, 6011–6013; d) Y. Oaki, H. Imai, *J. Mater. Chem.* **2007**, *17*, 316–321.

Received: March 29, 2007
Revised: June 9, 2007
Published online: July 23, 2007

